Processing and Application of Ceramics 14 [2] (2020) 91–101
https://doi.org/10.2298/PAC2002091L

Effects of molar ratio on dielectric, ferroelectric and magnetic properties of $Ni_{0.5}Zn_{0.5}Fe_2O_4$-$BaTiO_3$ composite ceramics

Xiaodong Luo[1,2,3,*], Hong Wang[2], Rongli Gao[2,3], Xinliang Li[2], Jing Zhang[1,4,*], Heng Ban[5]

[1]*College of Materials Science and Engineering, Chongqing University, Chongqing 400044, China*
[2]*School of Metallurgy and Materials Engineering, Chongqing University of Science and Technology, Chongqing 401331, China*
[3]*Chongqing Key Laboratory of Nano/Micro Composite Materials and Devices, Chongqing 401331, China*
[4]*National Engineering Research Center for Magnesium Alloys, Chongqing Universtiy, Chongqing 400044, China*
[5]*Department of Mechanical Engineering and Materials Science, University of Pittsburgh, PA 15260, USA*

Received 23 March 2019; Received in revised form 3 July 2019; Received in revised form 31 December 2019; Accepted 16 February 2020

Abstract

$Ni_{0.5}Zn_{0.5}Fe_2O_4$-$BaTiO_3$ (NZFO-BTO) magnetoelectric composite ceramics with different molar ratios (m_{NZFO}:m_{BTO} = 1:1.5, 1.5:1 and 2:1, defined as $N_1B_{1.5}$, $N_{1.5}B_1$ and N_2B_1, respectively) were prepared successfully by using a joint hydrothermal method and sol-gel technique and sintering at 1000 °C. Meanwhile, the dielectric, ferroelectric and magnetic properties of the composites were investigated. The presence of bi-phase structure in the composites was verified with X-ray diffraction analyses. The scanning electron microscopy images and energy dispersion spectrum results confirmed that the bulk-like grains (2 to 5 μm) and sphere-like grains (~0.5 μm) could be attributed to NZFO and BTO, respectively. The dielectric constant and loss increased with increasing NZFO/BTO molar ratio because the carrier concentration of NZFO is higher than that of BTO. Thus, the dielectric constant of the N_2B_1 ceramics is more than 7800 at low frequency of 100 Hz and room temperature, while only less than 2000 for the $N_1B_{1.5}$ composite. Two peaks can be observed in the temperature dependence of the dielectric constant curves. One is near 120 °C, which corresponds to the Curie temperature of BTO, while the other peak occurs at about 320 °C, corresponding to the relaxation polarization. The remanent polarization increases with increasing the content of ferroelectric BTO. The maximum value at 1 kHz was observed for the $N_1B_{1.5}$ sample and it is larger than 4.5 μC/cm^2, while the minimal value was obtained for the N_2B_1 composite and is only 1.2 μC/cm^2. Magnetic properties were also measured and it was observed that magnetization increases with increasing the molar ratio. The largest saturation magnetization has the N_2B_1 composite (~51.74 emu/g) due to the larger concentration of NZFO phase. However, the sample $N_1B_{1.5}$ shows the largest coercive field due to the highest interface interaction. This study provides guidelines for the fabrication of NZFO-BTO magnetoelectric composite ceramics.

Keywords: *molar ratio, NZFO-BTO, magnetoelectric composite ceramics*

I. Introduction

Multiferroic materials with excellent physical properties attract tremendous interest from both scientific research and their potential applications point of view, such as in spintronics, novel energy storage devices, sensors, capacitors etc. [1–3]. Especially, multiferroic materials simultaneously show magnetic and ferroelectric ordering and they can be coupled with each other, i.e. the magnetic properties can be tuned by electric field and vice versa, this is called magnetoelectric coupling (MEC) effect. Many new functional devices can be explored based on this MEC effect.

Single phase multiferroic materials are limited in

* Corresponding author: tel: +86 13637992925,
e-mail: *lxd336@cqust.edu.cn* (Xiaodong Luo)
jingzhang@cqu.edu.cn (Jing Zhang)

practical applications, since their magnetic and ferroelectric Curie temperatures are much lower than room temperature [4–6]. Although $BiFeO_3$, as a typical room temperature single phase multiferroic material, has the ferroelectric ($T_C \sim 1103$ K) and antiferromagnetic ($T_N = 643$ K) transition temperatures far above room temperature, the MEC effect of $BiFeO_3$ is still very weak. This is mostly because of its weak magnetization induced by the G-type antiferromagnetic spiral structure coupled with serious leakage current generated by the impurities and defects such as oxygen vacancies and the change in the valence of iron $Fe^{3+} \rightarrow Fe^{2+}$ [7–9]. Multiferroic properties at room temperature have recently been discovered in barium hexaferrites doped with diamagnetic cations [10]. Herewith the magnetoelectric characteristics of M-type hexaferrites fabricated by a modified ceramic technique are more advanced than those for the well-known room temperature $BiFeO_3$ orthoferrite multiferroic. This is the simplest type of all ferrites with a hexagonal structure. More than 90% of permanent magnets are produced all over the world based on this compound. This compound is a deep semiconductor ($\sim 10^9$ Ω·cm) at room temperature with a ferrimagnetic structure and a total magnetic moment of $20\,\mu_B$ in the ground state [11]. However, the observed multiferroic coupling is limited. Therefore, it is a long-term and arduous challenge to overcome the difficulties of weak MEC effect in the single phase materials and to exploit new functional materials with strong MEC effect.

Fortunately, this limitation of MEC effect of the single phase multiferroic materials may be overcome in multiphase composite multiferroic materials, which take advantage of the specific coupling between the individual components to obtain properties that are absent in the individual constituent phases [12–14]. A generally accepted result of MEC effect in composite multiferroic materials is the product of the magnetostrictive effect in the magnetic phase and the piezoelectric effect in the ferroelectric phase [15–17]. According to this statement, the most probable approach to obtain strong MEC effect is coupling of the interfacial stress between the ferroelectric and magnetic phases to an extreme [18–20]. It is quite clear that the coupling effect of multiferroic composite materials depends greatly on the properties of component phases, such as the magnetostrictive/ piezoelectric coefficient, magnetization/polarization and the coercive magnetic/electric field of the magnetic/ferroelectric phases. Actually, in order to obtain excellent multiferroic properties in magnetoelectric composites, good ferromagnetic nature, i.e. large total magnetic moment at operating temperature (ambient temperature) is also very important.

Till now, several composites have been investigated. For example, $Ba(Sr,Ti)O_3$, $BiFeO_3$, $Pb(Zr,Ti)O_3$ and PMN-PT were generally chosen as the ferroelectric phases, while $(La,Sr)MnO_3$, $(La,Ca)MnO_3$, NZFO, MFe_2O_4 (M = Co, Ni, Cu, Zn, Mg, Ca, etc.), Terfenol-D and Fe_3O_4 were treated as the magnetic phases [16–25]. However, in addition to the respective properties of the component phase, the geometrical phase arrangement in such composites has significant effect on the coupling effect. It is probably worth pointing out that the composite in the form of uniformly distributed geometry is expected to show improved coupling effect due to its better phase connectivity, high insulation and larger interface area. Also, it can overcome the drawbacks of thermal expansion, grain boundary and so forth [26–28]. In addition, the magnetoelectric composites with proper molar ratio between the two phases are also anticipated to present enhanced coupling effect due to its better balanced properties between the two phases, that is, proper magnetic and ferroelectric properties can be acquired. Therefore, it is necessary to investigate the effect of molar ratio on MEC effect in magnetoelectric composites. However, it was reported that thickness, width and length of fractions strongly influence the maximum ME coefficient. Clearly, geometry effects cannot be ignored in prediction of ME coefficient.

Herein, ferrite NZFO was used for the magnetic phase. It is a widespread magnetic component due to its strong magnetostriction and high resistance and thus strong coupling effect and excellent insulation of the composites can be expected. $BaTiO_3$ (BTO) was selected as the ferroelectric phase because of its excellent piezoelectric properties. Hydrothermal method combined with sol-gel method was used to prepare the composite ceramics in order to improve the dispersity. Correspondingly, we make an attempt to explore the effects of molar ratio of NZFO to BTO (1:1.5, 1.5:1 and 2:1) on the structure, dielectric, ferroelectric and magnetic properties of NZFO-BTO based magnetoelectric composite multiferroics.

II. Experimental procedure

2.1. Synthesis of NZFO-BTO composite particles

All chemical reagents used in this study were purchased from Sinopharm Chemical Regent Beijing Co. Ltd., including ferric trichloride ($FeCl_3 \cdot 6\,H_2O$), sodium hydroxide (NaOH), ethylene glycol (EG), ethanol (C_2H_6O), barium acetate ($Ba(CH_3COO)_2$), glacial acetic acid (CH_3COOH), titanium butoxide ($TiC_{12}H_{28}O_4$), 2-ethoxyethanol ($C_4H_{10}O_2$). All of these reagents are used without further purification.

Stoichiometric amounts of $Ni(NO_3)_2 \cdot 6\,H_2O$, $ZnCl_3 \cdot 6\,H_2O$ and $FeCl_3 \cdot 6\,H_2O$ together with NaOH (using the molar ratio of 2:1) were dissolved in 70 ml of EG and stirred constantly to make uniform mixture. The mixed solution was then sealed in a 100 ml Teflon-lined stainless steel autoclave, heated in a vacuum drying oven while the temperature was maintained at 200 °C for 10 h. After the hydrothermal treatment, it was cooled down to room temperature naturally. The obtained black product was washed with ethanol and deionized water for several times, and then it was dried

in a vacuum oven at 80 °C for 10 h.

In the next step, $C_4H_{10}O_2$ and CH_3COOH with the volume ratio of 4:1 were mixed and then NZFO was dispersed into the mixed solvent with constant stirring and sonic oscillation for 10 min. Subsequently, $Ba(CH_3COO)_2$ was dissolved in the mixed solvent to form Ba precursor solution, stirred well and heated at 70 °C for 30 min to make sure that $Ba(CH_3COO)_2$ is dissolved completely. Then, $TiC_{12}H_{28}O_4$ was mixed with Ba precursor solution and stirred constantly for 30 min to form the mixture. The pH value of the precursor solution is adjusted to be about 3 by adding $HOCH_2CH_2NH_2$. Then $CH_3COCH_2COCH_3$ was added to control the hydrolysis rate. The concentration of the precursor solution was subsequently adjusted to 0.3 mol/l by adding a certain amount of $C_4H_{10}O_2$. Finally, the solution was heated and continuously stirred, resulting in the gelation of BTO on the surface of the NZFO nanoparticles. The obtained composite sol was heated at 80 °C to form a gel followed by a heat treatment at 800 °C to burn out the organic solvent and form NZFO-BTO composite particles with different molar ratios of ferrite and titanate phases (m_{NZFO}:m_{BTO} = 1:1.5, 1.5:1 and 2:1, defined as $N_1B_{1.5}$, $N_{1.5}B_1$ and N_2B_1, respectively).

2.2. Preparation of NZFO-BTO composite ceramics

NZFO-BTO magnetoelectric composite ceramics with different molar ratios were prepared successfully by using a joint hydrothermal method and sol-gel technique (Fig. 1). Firstly, the NZFO-BTO composite particles were added into distilled water and then ball milled for 8 h by the planetary ball mill (XQM-4, Tencan powder Co. Ltd, China). After that the obtained slurries were dried at 120 °C. The composite particles were pressed at 12 MPa into pellets with the diameter of 10 mm and the thickness of 1 mm and then the pressed samples were sintered at 1000 °C for 2 h in a chamber furnace (KBF1700, Nanjing Nanda instrument plant, China). For the measurement of electric properties and to avoid the short circuit, the sintered samples were polished, and then conductive silver paste was respectively pasted on the upper and lower surfaces in the centre to form two circular electrodes with the diameter of 6 mm. Then they were burned at 500 °C for 30 min so as to reduce the contact resistance between the sample and the electrodes and therefore Ohm contact may be expected. In this work, five samples of each composite mixture were tested.

2.3. Characterization

Structural analysis by X-ray diffraction (XRD) was performed using a D/max 2500 (Rigaku, Japan) with Cu-Kα_1 radiation (λ = 1.5406 Å). Scanning electron microscope (FE-SEM, JSM-7800F, JEOL, Japan) was used to check the surface morphology. The dielectric properties of the samples were measured by using an impedance analyser (HP4980A, Agilent, USA) combined with a high temperature system (TZDM-RT-1000, China). The relative dielectric constant (ε_r) can be calculated according to the following equation:

$$\varepsilon_r = \frac{C \cdot d}{\varepsilon_0 \cdot S} \tag{1}$$

where C, d and ε_0 are the capacitance, the thickness of the samples and the vacuum dielectric constant (8.85×10^{-12} F/m), S is the effective electrode area on the sample. The ferroelectric properties were measured by ferroelectric test system (TF2000, aix-ACCT Inc., Germany). Magnetic hysteresis loops were measured at room temperature using a vibrating sample magnetometer (VSM).

III. Results and discussion

3.1. Structure of prepared composites

X-ray diffraction patterns of the prepared NZFO-BTO ceramics with different molar ratios are shown in Fig. 2. It can be seen that the diffraction peaks could be

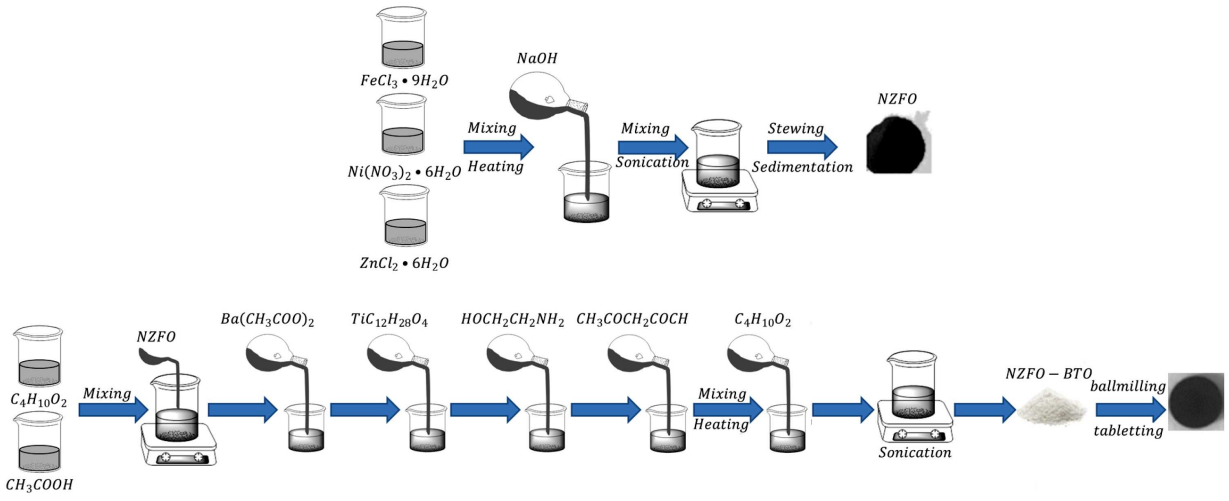

Figure 1. Schemes of the process for the fabrication of NZFO-BTO composites

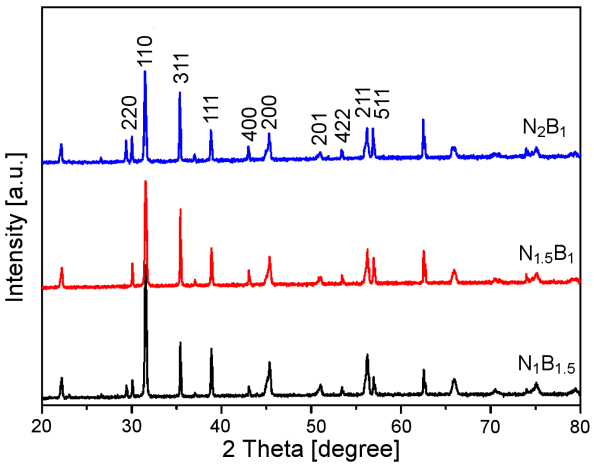

Figure 2. XRD patterns of NZFO-BTO composite ceramics with different molar ratios

indexed to (220), (311), (400), (422), (511) and (440) planes of NZFO, while the remaining peaks are identified as (110), (111), (200), (201), (211) and (220) planes of BTO. This clearly shows that there is no obvious chemical reaction between NZFO and BTO phases in the composite samples, and with this resolution limit of XRD, no obvious impurity phase peak can be observed. In addition, we note that with increasing the amount of ferroelectric phase, the intensities of the diffraction peaks of NZFO phase become weaker while those of BTO phase slightly increases accordingly. The relative intensity of the diffraction peaks between NZFO and BTO varies monotonically with the molar ratio, indicating the increased concentration of BTO in the composites with molar ratio decreased.

The SEM images of the NZFO-BTO composite ceramics with different molar ratios are shown in Fig. 3. It can be seen that all samples were composed of two

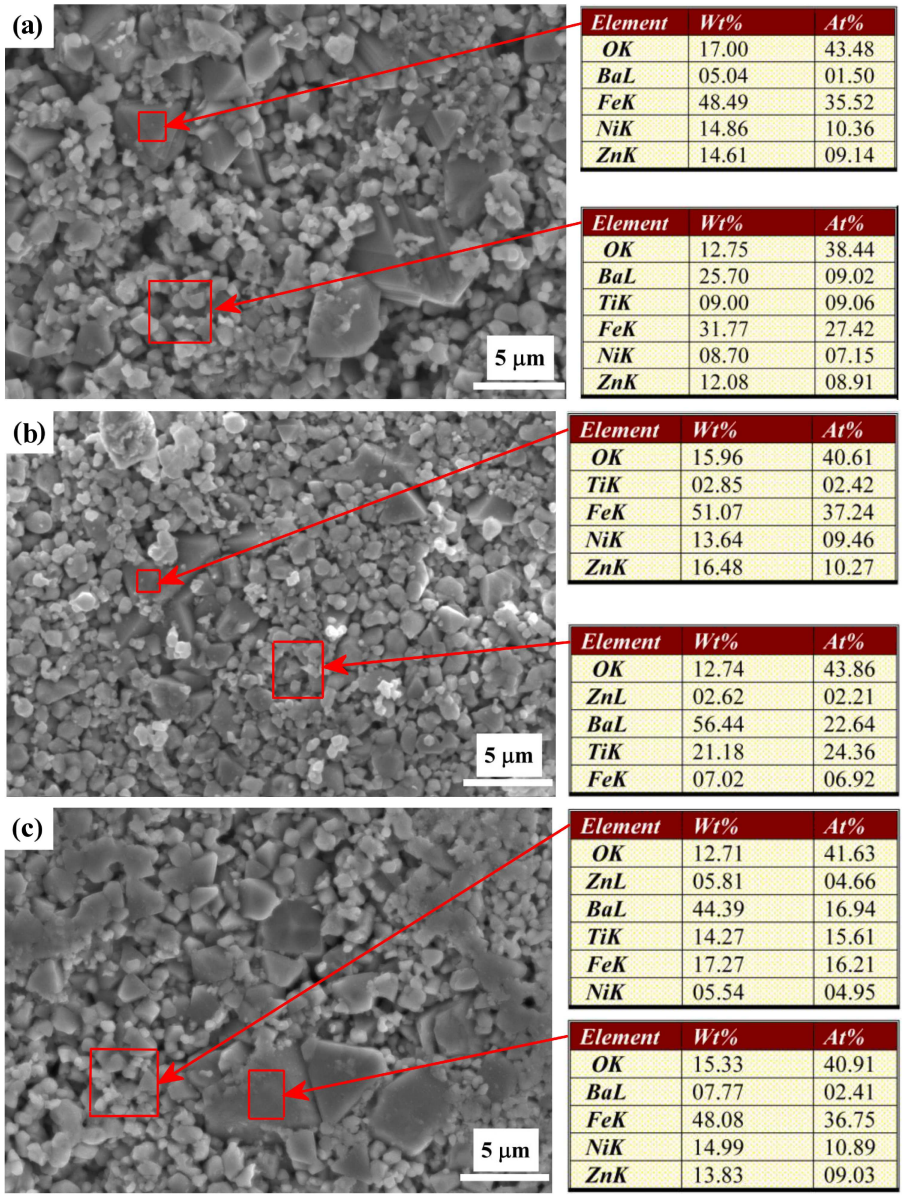

Element	Wt%	At%
OK	17.00	43.48
BaL	05.04	01.50
FeK	48.49	35.52
NiK	14.86	10.36
ZnK	14.61	09.14

Element	Wt%	At%
OK	12.75	38.44
BaL	25.70	09.02
TiK	09.00	09.06
FeK	31.77	27.42
NiK	08.70	07.15
ZnK	12.08	08.91

Element	Wt%	At%
OK	15.96	40.61
TiK	02.85	02.42
FeK	51.07	37.24
NiK	13.64	09.46
ZnK	16.48	10.27

Element	Wt%	At%
OK	12.74	43.86
ZnL	02.62	02.21
BaL	56.44	22.64
TiK	21.18	24.36
FeK	07.02	06.92

Element	Wt%	At%
OK	12.71	41.63
ZnL	05.81	04.66
BaL	44.39	16.94
TiK	14.27	15.61
FeK	17.27	16.21
NiK	05.54	04.95

Element	Wt%	At%
OK	15.33	40.91
BaL	07.77	02.41
FeK	48.08	36.75
NiK	14.99	10.89
ZnK	13.83	09.03

Figure 3. SEM images of the sintered composites: a) $N_1B_{1.5}$, b) $N_{1.5}B_1$ and c) N_2B_1, with compositions of the selected regions determined by EDS

kinds of grains. One is fine grained with the size of about 500 nm, and the other is larger with the size of more than 2 μm. In addition, the larger grains are strip-type with the length of more than 4 μm when the molar ratio is 1:1.5, as shown in Fig. 3a. When the molar ratio is 1.5:1, the larger grain is polygonal and the mean size is above 2 μm, as depicted in Fig. 3b. In contrast, it can be found in Fig. 3c that the larger grain shape becomes blocky when the molar ratio is 2:1. In addition, it is very obvious that the content of smaller grains decreases monotonically with the molar ratio increase, indicating that the larger grains are magnetic NZFO particles, while the smaller grains belong to BTO. Moreover, the average grain sizes of the smaller grains in the ceramics mainly remain the same while the larger grain sizes of the specimen decrease at first and then increase with the molar ratios. This means that appropriate addition of NZFO into BTO or addition of BTO into NZFO do not only change the grain shape, but also inhibit the grain growth and so refine the grains. This result indicates that the microstructure features, such as the grain size, grain shape and the density can be effectively manipulated by the recombination of magnetic and ferroelectric phases, implying the possibility to optimize the macroscopic performance by the approach of composition.

Energy dispersive X-ray spectroscopy (EDS) was used to confirm the composition of large and small grains in the NZFO-BTO composites. It is found that the Ni, Zn, Fe and O elements are primary for the particles with the large grain size, while Ba, Ti and O are the main elements when the grain is small (Fig. 3a). Similarly, it can be seen from Fig. 3b that that the major elements of the smaller grains are Ba, Ti and O, thus these particles with smaller size can be regarded as BTO. Furthermore, Ni, Zn, Fe, Ti and O are the main elements for the bigger particles, as shown in Fig. 3c. Although Ti element is observed in these particles, the reason can be ascribed to the large scanning volume of EDS where the marginal and overlapped BTO particles have been measured. But on the whole, these bigger particles are mainly categorized as NZFO phase. It can be seen from the images that the distribution of NZFO and BTO is relatively non-uniform, some agglomerations are formed, which may be due to the poor dispersion of NZFO in BTO precursor solution.

3.2. Dielectric and ferroelectric properties

The frequency dependencies of relative dielectric constant (ε_r) and loss ($\tan\delta$) at room temperature for the prepared ceramics are shown in Fig. 4. One can see from Fig. 4a that the dielectric constant of all the samples decreases sharply with the increase of frequency in the low frequency range, while the dielectric constant tends to be stable at higher frequencies. This can be attributed to the different responses of various polarization mechanisms in different frequency regions, and the polarization relaxation is ascribed to this phenomenon [29,30]. In general, the polarization mechanism of ferroelectric materials includes displacement polarization, turning-direction polarization and space charge polarization [31]. Among them, the response time of displacement polarization is very short ($\sim 10^{-13}$ s), therefore this polarization process can be entirely developed in the measured frequency range. However, the time for forming the turning-direction polarization and space charge polarization is very long ($\sim 10^{-5}$ s) compared with displacement polarization, therefore, these relaxation polarizations can only be developed when the frequency is very low.

In the low frequency range, if the resistance of the grain boundaries is high enough, electrons can accumulate at the grain boundaries because of thermal motion or field stress and thus polarization is produced. Whereas, with the increase of frequency, the pile up effect is reduced because electrons keep on switching their direction of motion and hence the polarization decreases. Another factor contributing to the permittivity at lower frequencies is the space charge polarization due to the inhomogeneous dielectric structure and other im-

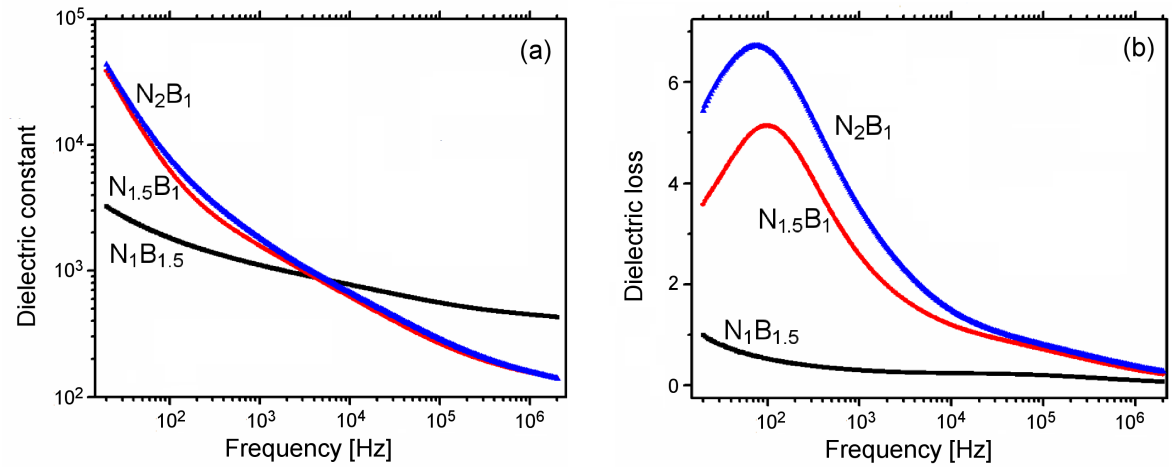

Figure 4. Frequency dependencies of dielectric properties at room temperature of NZFO-BTO composite ceramics with different molar ratios: a) dielectric constant and b) dielectric loss

perfections, such as the existence of impurities, porosity and grain structure [32–34]. When a small amount of free charges stays in the centre of the boundary surface to neutralize each other, a space charge layer will be formed and thus the space field can be changed, which is equivalent to increasing the dielectric properties. At relatively high frequencies, except for the displacement polarization, both the turning-direction and space charge polarizations cannot be produced. Therefore, the dispersion in dielectric constant becomes small and present frequency-independent response. In a word, the phenomenon of the dispersion in dielectric constant is explained on the basis of polarization mechanisms at different frequencies.

Furthermore, one can note that in the variation of dielectric constant with frequency there is an intersection line at about 5000 Hz. This result can be attributed to the different contributions of polarizations under different frequencies. The relaxation polarization for the $N_1B_{1.5}$ composite may be dominant in low frequency region. The mechanisms of slow polarization relaxation come from the diffuse of space charges and traps, indicating the different microstructure between the two specimens. As mentioned above, the inhomogeneity exists due to

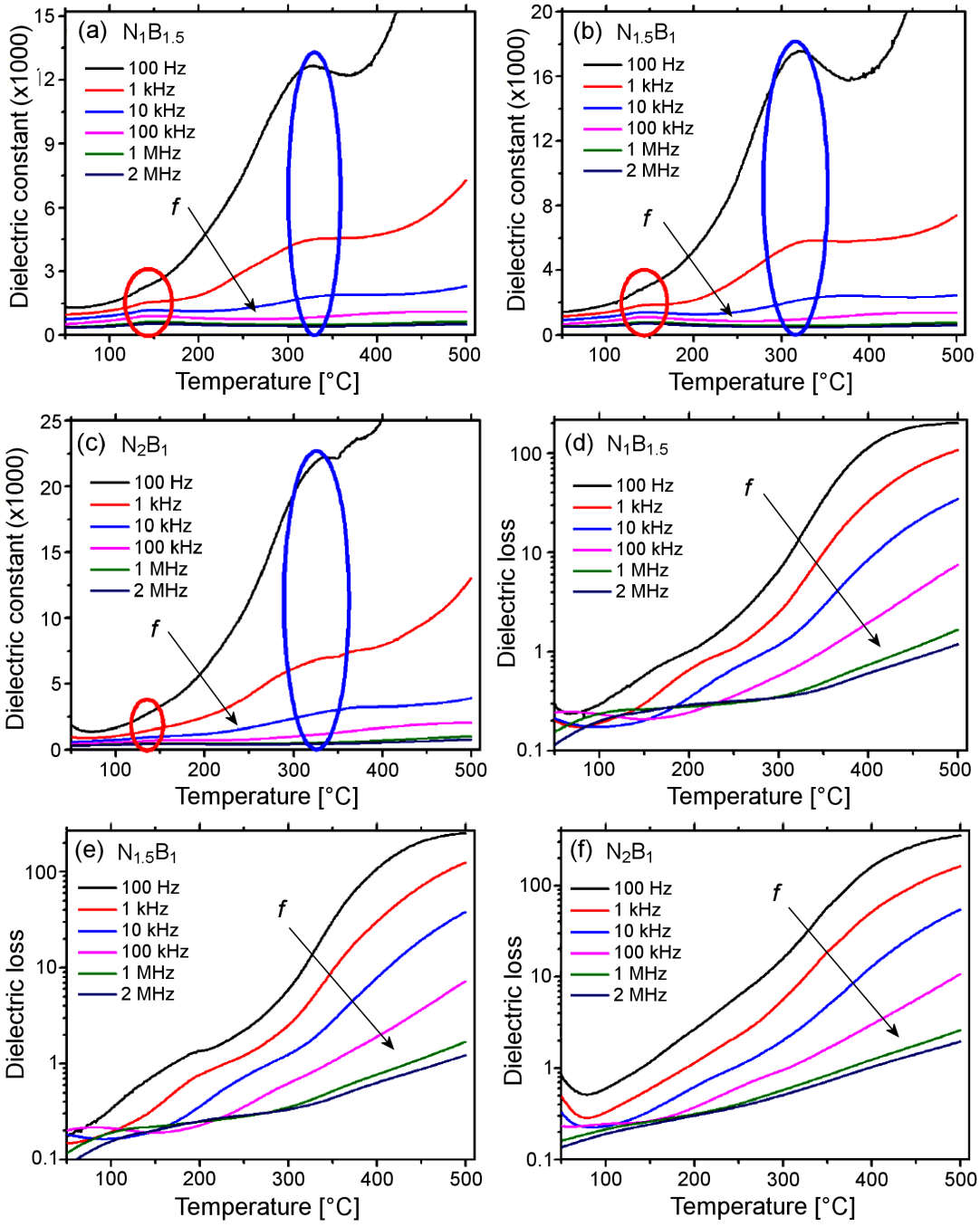

Figure 5. Temperature dependence of dielectric constant for: a) $N_1B_{1.5}$, b) $N_{1.5}B_1$ and c) N_2B_1 ceramics and dielectric loss for: d) $N_1B_{1.5}$, e) $N_{1.5}B_1$ and f) N_2B_1 ceramics

the impurities, porosity and grain structure, which intensifies the assembling of electrons at the interface, leading to an enhanced interface polarization. Besides, the grain size of the ceramics is different, and the size effect may lead to this phenomenon to some extent. This result indicates that the slow polarization mechanism is the major contribution of BTO in the low frequency range, signifying that the space charges may increase with the BTO content increasing.

Nevertheless, the dielectric loss measured at room temperature shows different variation tendency from that of the dielectric constant, as shown in Fig. 4b. It is worth noting that the dielectric loss for the $N_1B_{1.5}$ composite is the smallest as a whole, which can be ascribed to the minor space charges because of its better frequency stability of dielectric constant. The SEM images can also indicate more homogeneous structure as well as smaller grain size of BTO.

Figure 5 shows the temperature dependence of ε_r and tan δ of the prepared ceramics measured at different frequencies. It can be seen that the dielectric constant and loss of the composites do not change monotonically with the temperature. Thus, a maximal ε_r value occurs at about 350 °C for the frequency of 100 Hz, and the dielectric peak shifts to high temperature range with increasing the frequency, while the peak height decreases with the frequency. As it was discussed above, the peak may be related to the relaxation polarization induced by space charge or oxygen vacancies [35–37]. In the high temperature range, the dielectric constant and loss increase rapidly with the temperature. This is related to the increased electronic conduction because more and more electrons can be excited and migrate from valence band to conduction band. As a consequence, more electrons will accumulate at the grain boundary and thus polarization can be enhanced. Simultaneously, the dielectric loss also increases as a result of the increased conductivity.

Compared with the composite $N_1B_{1.5}$ (Fig. 5a), the peak for the sample $N_{1.5}B_1$ becomes dimmer in the high frequency range (Fig. 5b). The dielectric constant of the N_2B_1 composite increases also quickly with temperature, but the dielectric peak cannot be detected, as shown in Fig. 5c. In addition, the dielectric constant of the composite $N_1B_{1.5}$ at 250 °C is less than 9000 at the frequency of 100 Hz, correspondingly, the dielectric loss is about 2. Similarly, the constants of the composites $N_{1.5}B_1$ and N_2B_1 are more than 10000 and 12000, respectively. However, the dielectric loss does not show obvious variation being ~2 at 250 °C for all the samples. It should be pointed out that in the high temperature range, all the dielectric constants increase promptly with temperature and this may be related to the space charge polarization. As it has been mentioned before that more space charges can be excited if the temperature is high enough, in addition, with the increase of temperature, more and more electrons can be stimulated from the valence band to the conduction band, therefore, the large dielectric constant can be generated.

Furthermore, another dielectric loss peak can be observed for all the samples at about 400 °C. The peak position also shifts to higher temperature range with the increase of frequency. As it was indicated above, that the peak corresponding to the low temperature can be attributed to the relaxation loss which is caused by slow polarization process such as turning-direction polarization and space charge polarization. The high temperature loss peak may be related to the phase transition of NZFO.

In order to elucidate how the molar ratio affects the ferroelectric properties, the *P-E* curves of all the samples (Fig. 6) were measured at the same frequency (1 kHz). Obviously, although the coercive field (E_c) of all the specimens is nearly the same (~15 kV/cm), the remanent polarization (P_r) decreases with increasing the molar ratio. The maximal value of P_r is 4.5 μC/cm^2 obtained for the sample $N_1B_{1.5}$, while the specimen N_2B_1 has the minimum P_r of 1.2 μC/cm^2. Theoretically,

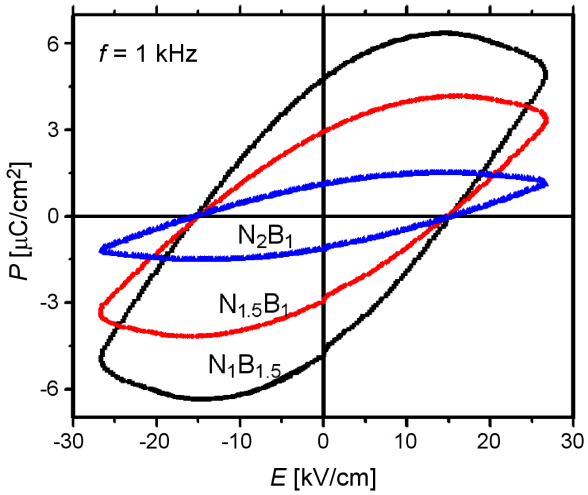

Figure 6. *P-E* curves of NZFO-BTO composite ceramics with different molar ratios

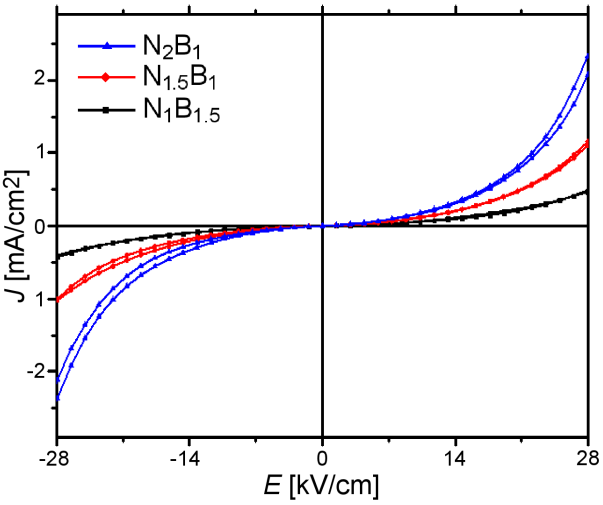

Figure 7. *J-V* curves of NZFO-BTO composite ceramics with different molar ratios

the remanent polarization of the composites should decrease with decreasing the content of ferroelectric phase.

Typical *J-V* curves indicate that the current density increases monotonically with the molar ratio increase, as shown in Fig. 7. When the applied bias field is 28 kV/cm, the values of current density for the samples $N_1B_{1.5}$, $N_{1.5}B_1$, and N_2B_1 are 0.4, 0.9 and 2.2 mA/cm^2, respectively. Although many factors can affect the leakage current, including defects, such as oxygen vacancies, grain boundaries, pores and interface, these elements may not be dominant. The reason for the enormous difference in the leakage current of these samples is that the carrier concentration in NZFO is much higher than that in BTO due to its smaller band gap. Therefore, the conductivity of NZFO is larger than that of BTO. As a consequence, by combining the *P-E* curves with *J-E* curves, it can be concluded that the sample $N_1B_{1.5}$ shows better ferroelectric properties.

3.3. Magnetic properties

The magnetic hysteresis loops of all composite ceramics are shown in Fig. 8. It is interesting to observe a clear hysteresis loop for the NZFO-BTO magnetoelectric composite ceramics, with very small coercive magnetic field (H_c), representing typical superparamagnetic character. The values of the saturation magnetization (M_s) for all the samples can be determined by the extrapolation of the magnetization curve to zero applied fields, and the magnetic parameters are listed in Table 1. It is obvious that both the remanent (M_r) and saturation magnetization (M_s) increase with the increase of molar ratio, i.e. with increasing the concentration of magnetic NZFO phase. However, H_c presents the opposite behaviour.

Table 1. Magnetic parameters of NZFO-BTO composite ceramics

Sample	$N_1B_{1.5}$	$N_{1.5}B_1$	N_2B_1
M_s [emu/g]	30.01	41.81	51.74
M_r [emu/g]	0.78	0.98	1.25
H_c [Oe]	33.07	30.86	28.98
M_{s-N} [emu/g]	75.02	69.68	77.61
Loss [emu/g·Oe]	1422	2050	2362

Generally speaking, the magnetization of NZFO-BTO composite ceramics is entirely contributed by NZFO because BTO is a non-magnetic material. Therefore, the magnetization should be proportional to the mass fraction of NZFO in this composite ceramics if there is no interaction between the two phases, and without considering the size effect as well as the different shapes of NZFO in different samples. The mass fraction of NZFO (ϕ_{m-N}) can be expressed as:

$$\phi_{m-N} = \frac{m_N}{m_N + m_B} = \frac{M_N \times n_N}{M_N \times n_N + M_B \times n_B} \quad (2)$$

where m_N and m_B are the masses of NZFO and BTO in the composites, respectively, M_N and M_B are the molar masses of NZFO (~230) and BTO (~233), respectively, while n_N and n_B are the molar fraction of NZFO and BTO in the composites, respectively. Therefore, the effective saturation magnetization of NZFO (M_{s-N}) is calculated by:

$$M_{s-N} = \frac{M_s}{\phi_{m-N}} \quad (3)$$

where M_s is the saturation magnetization of NZFO/BTO composites obtained from the *M-H* curves. The mass fraction and effective saturation magnetization of NZFO are also listed in Table 1. It is very strange to find out that the effective saturation magnetization of NZFO in the samples is quite different. The effective saturation magnetization of NZFO for the sample $N_{1.5}B_1$ is the smallest (69.68 emu/g), while the largest value (77.61 emu/g) is obtained in the specimen N_2B_1. Because the measured magnetization is macroscopic property, not for one particle, therefore the abnormal result cannot be attributed to the heterogeneous distribution of the magnetic and ferroelectric phase. One possible reason for the disproportionate effective magnetization to

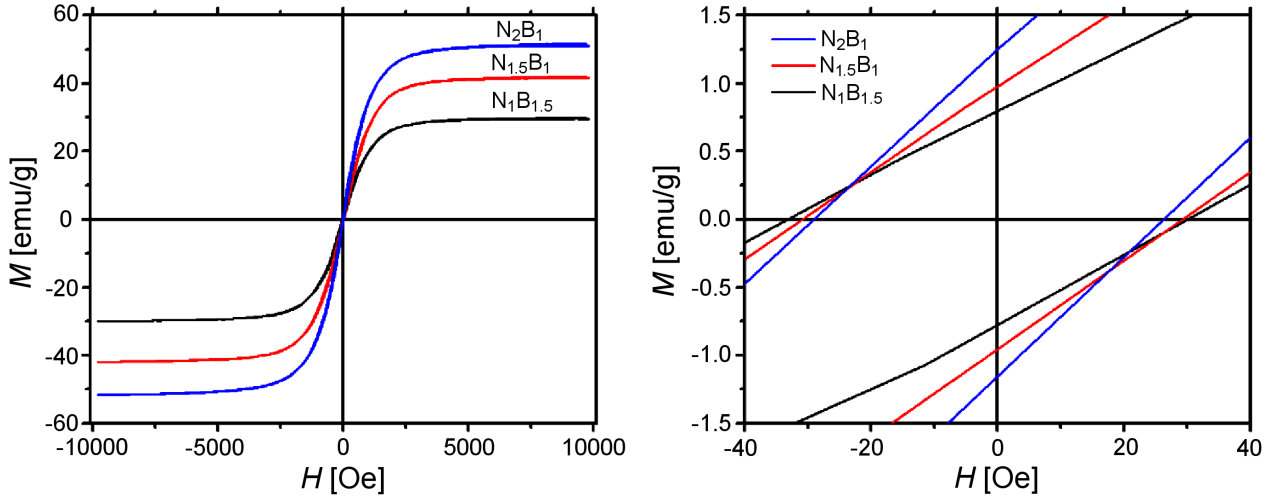

Figure 8. Room temperature *M-H* curves of NZFO-BTO composite ceramics with different molar ratios

molar ratio may be the presence of interface coupling effect between the two phases. Proper ratio between the two phases can induce the largest uncompensated spin magnetic moment and thus the reduced amount of magnetic phase can result in the enhancement of magnetic properties [37–39].

In general, the magnetization of the composite ceramics should be in direct proportion to the component of NZFO if there is no interface interaction between the two phases. However, the magnetization of the samples is highly deviated from the theoretical values. One reason may be attributed to the composite effect of large-scale cationic migration and surface spin disorder. The existence of non-magnetic perovskite phase BTO is likely to influence the magnetic properties of the composites because surface spin disorder is often associated with magnetic nanoparticles [40]. In these magnetoelectric composites, disorder at the surface may be due to the broken or unsaturated bonds, competing interactions or different grain boundary microstructures. The surface spin canting of magnetic nanoparticles is a natural consequence of surface spin disorder.

In addition, it is well known that the complex 3*d*-metal oxides easily allow the oxygen excess and/or deficit. Therefore, oxygen non-stoichiometry greatly affects the magnetic and magnetoelectric properties of complex oxides [41]. Oxygen excess and deficit can increase and decrease the oxidation degree of 3*d*-metals. The changing of charge state of 3*d*-metals as a consequence of the change of oxygen content alters such magnetic parameters as total magnetic moment and the Curie point. Moreover, oxygen vacancies have effect on exchange interactions. Intensity of exchange interactions decreases with oxygen vacancy concentration increase. In complex oxides there is only indirect exchange. Exchange near the oxygen vacancies is negative according to the Goodenough-Kanamori empirical rules. Oxygen vacancies should lead to the formation of a weak magnetic state such as spin glass.

It may also be observed from Table 1 that the coercivity (H_c) decreases with NZFO concentration in obtained materials. The highest H_c is 33.07 Oe when the ratio is 1:1.5 and it can be ascribed to the large grain size. In addition, it can be seen from Table 1 that the magnetic loss increases with increasing the content of NZFO in the composites. Although the value of H_c for the N_2B_1 composite is the lowest, it has the largest remanent magnetization and saturation magnetization, which results in the highest magnetic loss (2362 emu/g·Oe). In general, the magnetic loss in ferrite is mainly composed of residual loss and hysteresis loss. The hysteresis loss results from the irreversible magnetization in magnetic materials. In quasi-static magnetization, the magnetic loss is proportional to the area of hysteresis loop. In the magnetization cycle of AC magnetic field, there are not only eddy current loss, but also the acceleration of domain walls and the loss of elastic energy. Nevertheless, although the magnetic loss increases with increasing the content of NZFO, it is not in direct proportion to the mass fraction of NZFO in the composites. Therefore, the phenomenon should be related to the stronger interface interaction, thus the increased coercive field will affect the loss.

IV. Conclusions

NZFO/BTO magnetoelectric multiferroic materials with different NZFO/BTO molar ratios have been successfully prepared by combining hydrothermal method and sol-gel method. The formation of bi-phase magneto/electric structures after sintering at 1000 °C has been confirmed by XRD. All ceramics show dispersion in dielectric constants and both the dielectric constant and loss show non-monotonic variation with the increase of molar ratio. The sample $N_1B_{1.5}$, with NZFO/BTO molar ratio 1:1.5, possesses preferable ferroelectric properties and lower leakage current density compared to other samples due to the larger content of ferroelectric phase in the ceramics. The sample N_2B_1, with NZFO/BTO molar ratio 2:1, shows the strongest magnetization because of stronger interface interaction and the highest concentration of magnetic phase NZFO. Thus, these results may provide some valuable information for enhancing the magnetoelectric coupling effect of magnetoelectric composites.

Acknowledgement: This work has been supported by the National Natural Science Foundation of China (Grant Nos. 11647036), Scientific and Technological Research Program of Chongqing Municipal Education Commission (Grant No. KJ1713338), and the Scientific & Technological Achievements Foundation Project of Chongqing University of Science & Technology (Grant No. CK2017zkyb011). the Chongqing Research Program of Basic Research and Frontier Technology (CSTC2018jcyjAX0416, CSTC2016jcyjA0175, CSTC2016jcyjA0349), the Young Scientific and Technological Research Program of Chongqing Municipal Education Commission (KJQN201801509), the Excellent Talent Project in University of Chongqing (Grant No. 2017-35), the Science and Technology Innovation Project of Social Undertakings and Peoples Livelihood Guarantee of Chongqing (Grant No. cstc2017shmsA0192), and The Postgraduate science and technology innovation project of Chongqing University of Science & Technology (YKJCX1920215).

References

1. R.L. Gao, Y.S. Chen, J.R. Sun, Y.G. Zhao, J.B. Li, B.G. Shen, "Complex transport behavior accompanying domain switching in $La_{0.1}Bi_{0.9}FeO_3$ sandwiched capacitors", *Appl. Phys. Lett.*, **101** (2012) 152901.
2. H.T. Yi, T. Choi, S.G. Choi, Y.S. Oh, S.-W. Cheong, "Mechanism of the switchable photovoltaic effect in ferroelectric $BiFeO_3$", *Adv. Mater.*, **23** (2011) 3403.
3. R.L. Gao, C.L. Fu, W. Cai, G. Chen, X.L. Deng, H.R. Zhang, J.R. Sun, B.G. Shen. "Electric control of the Hall

effect in Pt/$Bi_{0.9}La_{0.1}FeO_3$ bilayers", *Sci. Rep.*, **6** (2016) 20330.
4. T. Zhao, A. Scholl, F. Zavaliche, K. Lee, M. Barry, A. Doran, M.P. Cruz , Y.H. Chu, C. Ederer, N.A. Spaldin, R.R. Das, D.M. Kim, S.H. Baek, C.B. Eom, R. Ramesh, "Electrical control of antiferromagnetic domains in multiferroic $BiFeO_3$ films at room temperature", *Nat. Mater.*, **5** (2006) 823–829.
5. R.L. Gao, H.W. Yang, C.L. Fu, W. Cai, G. Chen, X.L. Deng, J.R. Sun, Y.G. Zhao, B.G. Shen, "Tunable photovoltaic effects induced by different cooling oxygen pressure in $Bi_{0.9}La_{0.1}FeO_3$ thin films", *J. Alloy. Compd.*, **624** (2015) 1–8.
6. T. Choi, S. Lee, Y. Choi, V. Kiryukhin, S. Cheong, "Switchable ferroelectric diode and photovoltaic effect in $BiFeO_3$", *Science*, **324** (2009) 63–66.
7. R.L. Gao, H.W. Yang, Y.S. Chen, J.R. Sun, Y.G. Zhao, B.G. Shen, "Effect of cooling oxygen pressure on the photoconductivity in $Bi_{0.9}La_{0.1}FeO_3$ thin films", *J. Alloy. Compd.*, **591** (2014) 346–350.
8. Z.X. Li, Z. H. Wang, R.L. Gao, W. Cai, G. Chen, X.L. Deng, C.L. Fu, "Dielectric, ferroelectric and magnetic properties of $Bi_{0.78}La_{0.08}Sm_{0.14}Fe_{0.85}Ti_{0.15}O_3$ ceramics prepared at different sintering conditions", *Process. Appl. Ceram.*, **12** [4] (2018) 394–402.
9. R.L. Gao, H.W. Yang, J.R. Sun, Y.G. Zhao, B.G. Shen., "Oxygen vacancies induced switchable and nonswitchable photovoltaic effects in Ag/$Bi_{0.9}La_{0.1}FeO_3$/$La_{0.7}Sr_{0.3}MnO_3$ sandwiched capacitors", *Appl. Phys. Lett.*, **104** (2014) 031906.
10. S.V. Trukhanov, A.V. Trukhanov, V.G. Kostishyn, L.V. Panina, A.V. Trukhanov, V.A. Turchenko, D.I. Tishkevich, E.L. Trukhanova, V.V. Oleynik, E.S. Yakovenko, L.Yu. Matzui, D.A. Vinnik, "Magnetic, dielectric and microwave properties of the $BaFe_{12-x}Ga_xO_{19}$ ($x \leq 1.2$) solid solutions at room temperature", *J. Magn. Magn. Mater.*, **442** (2017) 300–310.
11. A.V. Trukhanova, S.V. Trukhanov, L.V. Panina, V.G. Kostishyn, D.N. Chitanov, I.S. Kazakevich, A.V. Trukhanov, V.A. Turchenko, M.M. Salem, "Strong corelation between magnetic and electrical subsystems in diamagnetically substituted hexaferrites ceramics", *Ceram. Int.*, **43** (2017) 5635–5641.
12. Y.Z. Xue, R.C. Xu, Z.H. Wang, R. L. Gao, C. Y. Li, G. Chen, X.L. Deng, W. Cai, C.L. Fu, "Effect of magnetic phase on structural and multiferroic properties of $Ni_{1-x}Zn_xFe_2O_4$/$BaTiO_3$ composite ceramics", *J. Electron. Mater.*, **48** [8] (2019) 4806–4817.
13. R.L. Gao, Q.M. Zhang, Z.Y. Xu, Z.H. Wang, W. Cai, G. Chen, X.L. Deng, X.L Cao, X.D. Luo, C.L. Fu., "Strong magnetoelectric coupling effect in $BaTiO_3$@$CoFe_2O_4$ magnetoelectric multiferroic fluids", *Nanoscale*, **10** (2018) 11750–11759.
14. X.F. Qin, R.C. Xu, H. Wu, R.L. Gao, Z.H. Wang, G. Chen, C.L. Fu, X.L. Deng, W. Cai, "A comparative study on the dielectric and multiferroic properties of $Co_{0.5}Zn_{0.5}Fe_2O_4$/$Ba_{0.8}Sr_{0.2}TiO_3$ composite ceramics", *Process. Appl. Ceram.*, **13** [4] (2019) 349–359
15. R.L. Gao, Q.M. Zhang, Z.Y. Xu, Z.H. Wang, G. Chen, X.L. Deng, C.L. Fu, W. Cai, "A comparative study on the structural, dielectric and multiferroic properties of $Co_{0.6}Cu_{0.3}Zn_{0.1}Fe_2O_4$/$Ba_{0.9}Sr_{0.1}Zr_{0.1}Ti_{0.9}O_3$ composite ceramics", *Composites Part B*, **166** (2019) 204–212.
16. R.C. Xu, S.L. Zhang, F.Q. Wang, Q.W. Zhang, Z.D. Li, Z.H. Wang, R.L. Gao, C.L. Fu, "The study of microstructure, dielectric and multiferroic properties of (1-x)$Co_{0.8}Cu_{0.2}Fe_2O_4$-x$Ba_{0.6}Sr_{0.4}TiO_3$ composites", *J. Electron. Mater.*, **48** [1] (2019) 386–400.
17. R.L. Gao, Q.M. Zhang, Z.Y. Xu, Z.H. Wang, G. Chen, C.L. Fu, X.L. Deng, W. Cai, "Anomalous magnetoelectric coupling effect of $CoFe_2O_4$-$BaTiO_3$ binary mixed fluids", *ACS Appl. Electron. Mater.*, **1** [7] (2019) 1120–1132.
18. L. Bai, R.L. Gao, Q.M. Zhang, Z.Y. Xu, Z.H. Wang, C.L. Fu, G. Chen, X.L. Deng, W. Cai, "Influence of molar ratio on dielectric, ferroelectric and magnetic properties of $Co_{0.5}Mg_{0.5}Fe_2O_4$/$Ba_{0.85}Sr_{0.15}TiO_3$ composite ceramics", *Process. Appl. Ceram.*, **13** [3] (2019) 257–268.
19. R.L. Gao, Q.Z. Leng, Z.H. Wang, G. Chen, C.L. Fu, X.L. Deng, W. Cai, "Magnetocapacitance and magnetoelectric coupling effect of $Ni_{0.5}Cu_{0.5}Fe_2O_4$/$BaTiO_3$ mixed multiferroic fluids", *Mater. Res. Express.*, **6** (2019) 026308.
20. S. Yi, R.C. Xu, X.F. Qin, H. Wu, X.L. Deng, R.L. Gao, Z.H. Wang, G. Chen, W. Cai, C.L. Fu, "Effect of molar ratio on the microstructure, dielectric and electromagnetic properties of $BaTiO_3$/$CoFe_2O_4$ ceramic", *Mater. Res. Express.*, **6** (2019) 116317.
21. R.L. Gao, Z.H. Wang, G. Chen, X.L. Deng, W. Cai, C.L. Fu, "Influence of core size on the multiferroic properties of $CoFe_2O_4$@$BaTiO_3$ core shell structured composites", *Ceram. Int.*, **44** (2018) S84–S87.
22. S.X. Dong, J.Y. Zhai, J.F. Li, D. Viehland, "Near-ideal magnetoelectricity in high-permeability magnetostrictive/piezofiber laminates with a (2-1) connectivity", *Appl. Phys. Lett.*, **89** [2] (2006) 52904.
23. R.L. Gao, L. Bai, Z.Y. Xu, Q.M. Zhang, Z.H. Wang, W. Cai, G. Chen, X.L. Deng, C.L. Fu, "Electric field-induced magnetization rotation in magnetoelectric multiferroic fluids", *Adv. Electron. Mater.*, *4* [6] (2018) 1800030.
24. R.V. Chopdekara, Y. Suzuki, "Magnetoelectric coupling in epitaxial $CoFe_2O_4$ on $BaTiO_3$", *Appl. Phys. Lett.*, **89** (20006) 182506.
25. R.L. Gao, X.F. Qin, Q.M. Zhang, Z.Y. Xu, Z.H. Wang, C.L. Fu, G. Chen, X.L. Deng, W. Cai, "A comparative study of the dielectric, ferroelectric and anomalous magnetic properties of $Mn_{0.5}Mg_{0.5}Fe_2O_4$/$Ba_{0.8}Sr_{0.2}Ti_{0.9}Zr_{0.1}O_3$ composite ceramics", *Mater. Chem. Phys.*, **232** (2019) 428–443.
26. R.C. Xu, Z.H. Wang, R.L. Gao, S.L. Zhang, Q.W. Zhang, Z.D. Li, C.Y. Li, G. Chen, X.L. Deng, W. Cai, C.L. Fu, "Effect of molar ratio on the microstructure, dielectric and multiferroic properties of $Ni_{0.5}Zn_{0.5}Fe_2O_4$-$Pb_{0.8}Zr_{0.2}TiO_3$ nanocomposite", *J. Mater. Sci. Mater. Electron.*, **29** (2018) 16226–16237.
27. R.L. Gao, Q.M. Zhang, Z.Y. Xu, Z.H. Wang, C.L. Fu, G. Chen, X.L. Deng, X.D. Luo, Y. Qiu, W. Cai, "Enhanced multiferroic properties of $Co_{0.5}Ni_{0.5}Fe_2O_4$/$Ba_{0.85}Sr_{0.15}TiO_3$ composites based on particle size effect", *J. Mater. Sci. Mater. Electron.*, **30** [11] (2019) 10256–10273.
28. N. Kumar, A. Shukla, R.N.P. Choudhary, "Structural, electrical and magnetic properties of $Bi(Ni_{0.45}Ti_{0.45}Fe_{0.10})O_3$", *J. Alloys Compd.*, **747** (2018) 895–904.
29. R.L. Gao, X.F. Qin, Q.M. Zhang, Z.Y. Xu, Z.H. Wang, C.L. Fu, G. Chen, X.L. Deng, W. Cai, "Enhancement of magnetoelectric properties of (1-x)$Mn_{0.5}Zn_{0.5}Fe_2O_4$-x$Ba_{0.85}Sr_{0.15}Ti_{0.9}Hf_{0.1}O_3$ composite ceramics", *J. Alloy.*

Compd., **795** (2019) 501–512.
30. L. Bai, R.L. Gao, Q.M. Zhang, Z.Y. Xu, Z.H. Wang, C.L. Fu, G. Chen, X.L. Deng, X.D. Luo, W. Cai, "Strong magnetic properties and enhanced coupling effect by tailoring the molar ratio in $BaTiO_3/Co_{0.5}Mg_{0.3}Zn_{0.2}Fe_2O_4$ composite ceramics", *J. Mater. Sci. Mater. Electron.*, **30** (2019) 11563–11575
31. L. Bai, R.L. Gao, Q.M. Zhang, Z.Y. Xu, Z.H. Wang, C.L. Fu, G. Chen, X.L. Deng, Y.Q. Luo, W. Cai, "Microstructure, dielectric and enhanced multiferroic properties of $Fe_3O_4/PbZr_{0.52}Ti_{0.48}O_3$ composite ceramics", *J. Mater. Sci. Mater. Electron.*, **30** [13] (2019) 12295–12306.
32. R.L. Gao, C.L. Fu, W. Cai, G. Chen, X.L. Deng, H.R. Zhang, J.R. Sun, B.G. Shen, "Anomalous Hall effect based on $Pt/Bi_{0.9}La_{0.1}FeO_3$ bilayers", *J. Appl. Phys.*, **55** (2016) 045801.
33. N. Kumar. A. Shukla. R.N.P. Choudhary, "Structural, electrical and magnetic characteristics of Ni/Ti modified $BiFeO_3$ lead free multiferroic material", *J. Mater. Sci. Mater. Electron.*, **28** (2017) 6673–6684.
34. A. Chaudhuri, K. Mandal, "Large magnetoelectric properties in $CoFe_2O_4$:$BaTiO_3$ core-shell nanocomposites", *J. Magn. Magn. Mater.*, **377** (2015) 441–445.
35. S. Singh, N. Kumar, A. Jha, M. Sahni, K. Sung, J.H. Jung, S. Chaubey, "Dielectric and impedance spectroscopy of $(Ba,Sm)(Ti,Fe)O_3$ system in the low-medium frequency range", *J. Mater. Sci. Mater. Electron.*, **26** (2015) 32–36.
36. M. Lorenz, G. Wagner, Ve. Lazenka, P. Schwinkendorf, H. Modarresi, M.J. Van Bael, A. Vantomme, K. Temst, O. Oeckler, M. Grundmann, "Correlation of magnetoelectric coupling in multiferroic $BaTiO_3$-$BiFeO_3$ superlattices with oxygen vacancies and antiphase octahedral rotations", *Appl. Phys. Lett.*, **106** (2015) 012905.
37. K.C. Verma, S. Singh, S.K. Tripathi, R.K. Kotnala, "Multiferroic $Ni_{0.6}Zn_{0.4}Fe_2O_4$-$BaTiO_3$ nanostructures: Magnetoelectric coupling, dielectric, and fluorescence", *J. Appl. Phys.*, **116** (2014) 124103.
38. S. Singh, N. Kumar, R. Bhargava, M. Sahni, K.D. Sung, J.H. Jung, "Magnetodielectric effect in $BaTiO_3/ZnFe_2O_4$ core/shell nanoparticles", *J. Alloy. Compd.*, **587** (2014) 437–441.
39. G. Sreenivasulu, M. Popov, F.A. Chavez, S.L. Hamilton, P.R. Lehto, G. Srinivasan, "Controlled self-assembly of multiferroic core-shell nanoparticles exhibiting strong magneto-electric effects", *Appl. Phys. Lett.*, **104** (2014) 052901.
40. L.P. Curecheriu, M.T. Buscaglia, V. Buscaglia, L. Mitoseriu, P. Postolache, A. Ianculescu, P. Nanni, "Functional properties of $BaTiO_3$-$Ni_{0.5}Zn_{0.5}Fe_2O_4$ magnetoelectric ceramics prepared from powders with core-shell structure", *J. Appl. Phys.*, **107** (2010) 104106.
41. M.A. Almessiere, Y. Slimani, H. Güngünes, A. Baykal, S.V. Trukhanov, A.V. Trukhanov, "Manganese/yttrium co doped strontium nanohexaferrites: Evaluation of magnetic susceptibility and Mossbauer spectra", *Nanomaterials*, **9** (2019) 1–18.